

---

# Adaptive Randomized Smoothing: Certifying Multi-Step Defences against Adversarial Examples

---

Saiyue Lyu<sup>1\*</sup>, Shadab Shaikh<sup>1\*</sup>, Frederick Shpilevskiy<sup>1\*</sup>, Evan Shelhamer<sup>2</sup>, Mathias Lécuyer<sup>1</sup>

<sup>1</sup>University of British Columbia, <sup>2</sup>Google DeepMind

{saiyuel, shadabs3, fshpil}@cs.ubc.ca, shelhamer@deepmind.com, mathias.lecuyer@ubc.ca

\* equal contribution

## Abstract

We propose Adaptive Randomized Smoothing (ARS) to certify the predictions of our test-time adaptive models against adversarial examples. ARS extends the analysis of randomized smoothing using  $f$ -Differential Privacy to certify the adaptive composition of multiple steps. For the first time, our theory covers the sound adaptive composition of general and high-dimensional functions of noisy input. We instantiate ARS on deep image classification to certify predictions against adversarial examples of bounded  $L_\infty$  norm. In the  $L_\infty$  threat model, our flexibility enables adaptation through high-dimensional input-dependent masking. We design adaptivity benchmarks, based on CIFAR-10 and CelebA, and show that ARS improves accuracy by 2 to 5% points. On ImageNet, ARS improves accuracy by 1 to 3% points over standard RS without adaptivity.

## 1 Introduction

Despite impressive accuracy, deep learning models still show a worrying susceptibility to adversarial attacks. Such attacks have been shown for a large number of tasks and models (Costa et al., 2023; Chakraborty et al., 2018), including areas where security and safety are critical such as fraud detection (Pumsirirat and Liu, 2018) or self-driving (Cao et al., 2021).

Several rigorous defences have been proposed to certify robustness. Randomized Smoothing (RS) (Lécuyer et al., 2019; Cohen et al., 2019) does so by averaging predictions over noisy versions of the input at test time, and as such can scale to large deep learning models. However, RS has its limitations: it is inflexible and either degrades accuracy or only certifies against small attacks.

To address these shortcomings and improve robustness, there has been a recent push to develop defences that adapt to inputs at test time Croce et al. (2022), including for RS (Alfarra et al., 2022a; Súkeník et al., 2021; Hong et al., 2022). Most such adaptive defences are heuristic, unproven, and subject to improved attacks (Croce et al., 2022; Alfarra et al., 2022a; Hong et al., 2022), running the risk of reverting to a hopeless cat and mouse game with attackers (Athalye et al., 2018; Tramer et al., 2020), or only provide limited adaptivity (Súkeník et al., 2021; Hong et al., 2022) and gain (§5).

We (re)connect RS to Differential Privacy (DP), after its abandonment for a tighter analysis via hypothesis testing (Cohen et al., 2019), and introduce **Adaptive Randomized Smoothing (ARS)** to provide test-time adaptivity while preserving rigorous bounds. Specifically, we analyze RS through the lens of  $f$ -Differential Privacy ( $f$ -DP), and use this connection to leverage a key strength of DP: the end-to-end analysis of multi-step adaptive computation using composition results (§2).

We use ARS to design two-step defence against  $L_\infty$  adversaries on image classification (Figure 1), which is a challenging setting for RS Blum et al. (2020). The first step computes an input mask that focuses on task-relevant information. This reduces the dimension of the input, which is then passed

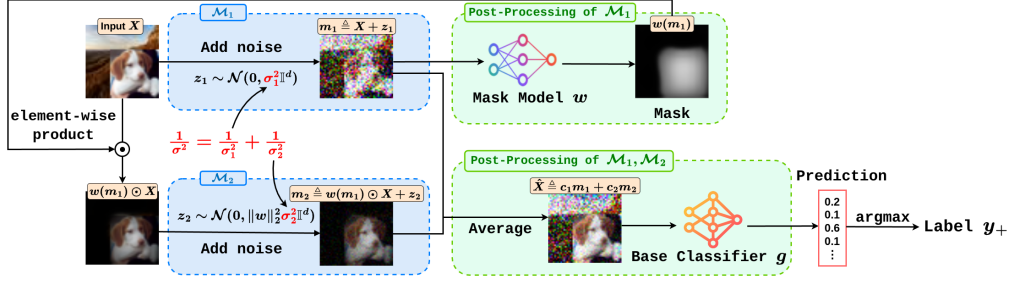


Figure 1: Two-step ARS for  $L_\infty$ -bounded attacks. Step  $\mathcal{M}_1$  adds noise to input  $X$  and post-processes the result into a mask  $w(m_1)$ . Step  $\mathcal{M}_2$  takes masked input  $w(m_1) \odot X$  and adds noise to get  $m_2$ . Base classifier  $g$  post-processes a weighted average of  $m_1, m_2$  to output a label. RS reduces to  $\sigma = \sigma$  and  $w(\cdot) = 1$  (no  $\mathcal{M}_1$ ).

to the second step for prediction. Thanks to this adaptive dimension reduction, the second step makes its prediction on a less noisy image, improving the performance and certification radius (§3).

We evaluate our adaptive randomized smoothing method in three settings (§4). For image classification, we first design a challenging benchmark based on CIFAR-10, and we show that ARS can improve accuracy by up to 9.9%. For spatially-localized face attribute classification on the CelebA dataset, we show that ARS improves accuracy by up to 10%. For large-scale image classification on ImageNet, ARS improves the accuracy by 1%. At radius 0.005, where RS has certified accuracy of 0 while ARS still has a certified accuracy of 15%.

## 2 Theory for Adaptivity via Differential Privacy

After introducing the necessary background and known results on RS and DP (§2.1), we reconnect RS to its DP roots by showing that the tight analysis of Cohen et al. (2019) can be seen as PixelDP (Lécuyer et al., 2019) using  $f$ -Differential Privacy (Dong et al., 2019; 2022), a hypothesis testing formulation of DP (§2.2). This connection lets us leverage composition results for  $f$ -DP to analyze multi-step approaches for provable robustness to adversarial examples, which we name Adaptive Randomized Smoothing (ARS) (§2.3). We leverage ARS to design and analyze a two-step defence against  $L_\infty$ -bounded adversaries (§2.4), which we then instantiate as a deep network (§3).

### 2.1 Related Work: Adversarial Robustness, Randomized Smoothing, and Differential Privacy

**Adversarial Examples (Szegedy et al., 2014):** Consider a classifier  $g : \mathcal{X} \rightarrow \mathcal{Y}$ , and input  $X$ . An adversarial example of radius  $r$  in the  $L_p$  threat model, for model  $g$  on input  $X$ , is an input  $X + e$  such that  $g(X + e) \neq g(X)$ , where  $e \in B_p(r)$ , where  $B_p(r) \triangleq \{x \in \mathbb{R}^d : \|x\|_p \leq r\}$  is the  $L_p$  ball of radius  $r$ . These inputs or attacks are made against classifiers at test time. For more on the active topics of attack and defence, we refer to surveys (Li et al., 2023; Costa et al., 2023; Chakraborty et al., 2018) on current attacks and provable defences. In general, provable defences do not focus on the largest-scale highest-accuracy classifiers, with the notable exception of randomized smoothing.

**Randomized Smoothing (RS) (Lécuyer et al., 2019; Cohen et al., 2019)** is a scalable approach to certifying model predictions against  $L_2$ -norm adversaries. Specifically, it certifies robustness to any attack  $\in B_2(r_X)$ . The algorithm randomizes a base model  $g$  by adding spherical Gaussian noise to its input, and produces a smoothed classifier that returns the class with highest expectation over the noise:  $y_+ \triangleq \arg \max_{y \in \mathcal{Y}} \mathbb{P}_{z \sim \mathcal{N}(0, \sigma^2 \mathbb{I}^d)}(g(X + z) = y)$ . The tightest analysis from Cohen et al. (2019) uses hypothesis testing theory to show that, with  $\underline{p}_+, \bar{p}_- \in [0, 1]$  such that  $\mathbb{P}(g(X + z) = y_+) \geq \underline{p}_+ \geq \bar{p}_- \geq \max_{y_- \neq y_+} \mathbb{P}(g(X + z) = y_-)$ , the certificate size  $r_X$  for prediction  $y_+$  is:

$$r_X = \frac{\sigma}{2} (\Phi^{-1}(\underline{p}_+) - \Phi^{-1}(\bar{p}_-)), \quad (1)$$

where  $\Phi^{-1}$  is the inverse standard Gaussian CDF,  $\underline{p}_+$  lower-bounds the probability of  $g(X + z) = y_+$  (the most probable class), and  $\bar{p}_-$  upper-bounds the probability of other classes.

While sound, RS is static during testing even though attacks may adapt. Recent work aims to make RS adapt at test time (Súkeník et al., 2021; Alfarra et al., 2022a; Hong et al., 2022). While pioneering, these works are restricted in either their soundness or their degree of adaptation and resulting improvement. Súkeník et al. (2021) soundly adapt the variance for RS by the distance between test and train inputs. However, this only provides minimal adaptivity, with only minor improvement to certification. Alfarra et al. (2022a) adapt the variance for RS to each test input, but the analysis is not end-to-end, and hence not sound (Súkeník et al., 2021). UniCR (Hong et al., 2022) adapts the noise distribution for RS, primarily to the data distribution during training, and optionally to input during testing. The train-time adaptation is sound, but the test-time adaptation is not due to the same issue raised by Súkeník et al. (2021). We propose ARS to advance certified test-time adaptivity: our approach is sound and high-dimensional to flexibly adapt the computation of later steps conditioned on earlier steps by differential privacy theory.

**Differential Privacy (DP)** is a rigorous notion of privacy. A randomized mechanism  $\mathcal{M}$  is  $(\epsilon, \delta)$ -DP if, for any neighbouring inputs  $X$  and  $X'$ , and any subset of possible outputs  $\mathcal{Y} \subset \text{Range}(\mathcal{M})$ ,  $\mathbb{P}(\mathcal{M}(X) \in \mathcal{Y}) \leq e^\epsilon \mathbb{P}(\mathcal{M}(X') \in \mathcal{Y}) + \delta$ . Following Lécuyer et al. (2019), we define neighbouring based on  $L_p$  norms:  $X$  and  $X'$  in  $\mathbb{R}^d$  are  $L_p$  neighbours at radius  $r$  if  $X - X' \in B_p(r)$ .

RS was initially analyzed using  $(\epsilon, \delta)$ -Differential Privacy (Lécuyer et al., 2019). Intuitively, the randomized classifier  $\mathcal{M}(X) \triangleq g(X + z)$ ,  $z \sim \mathcal{N}(0, \sigma^2 \mathbb{I}^d)$  acts as a privacy preserving mechanism (the Gaussian mechanism) that provably “hides” small variations in  $X$ . This privacy guarantee yields a robustness certificate for the expected predictions.

**$f$ -DP** (Dong et al., 2019) is a notion of privacy that extends  $(\epsilon, \delta)$ -DP, and defines privacy as a bound on the power of hypothesis tests. Appendix A provides more details on  $f$ -DP. The main result we leverage is Theorem 2.7 of Dong et al. (2022) that for a Gaussian mechanism  $\mathcal{M}(X) = \theta(X) + z$ ,  $z \sim \mathcal{N}(0, \frac{r^2}{\mu^2})$ , such that for any neighbouring  $X, X'$ ,  $\theta(X) - \theta(X') \in B_2(r)$  (i.e., the  $L_2$  sensitivity of  $\theta$  is  $r$ ), we have that  $\mathcal{M}$  is  $G_\mu$ -DP with:

$$G_\mu(\alpha) = \Phi\left(\Phi^{-1}(1 - \alpha) - \mu\right). \quad (2)$$

We leverage two key properties of  $f$ -DP. First,  $f$ -DP is resilient to post-processing. That is, if mechanism  $\mathcal{M}$  is  $f$ -DP,  $\text{proc} \circ \mathcal{M}$  is also  $f$ -DP. Second,  $f$ -DP is closed under adaptive composition. We refer to §3 in Dong et al. (2022) for the precise definition and use their Corollary 3.3: the adaptive composition of two Gaussian mechanisms  $G_{\mu_1}$ -DP and  $G_{\mu_2}$ -DP is itself  $G_\mu$ -DP, with:

$$\mu = \sqrt{\mu_1^2 + \mu_2^2} \quad (3)$$

$f$ -DP is distinct from the  $f$ -divergence from information theory. Dvijotham et al. (2020) use  $f$ -divergence bounds between the noise distribution centred on the original input and centred on any perturbed input. This improves RS by broadening the noise distributions and norm-bounds on the adversary that RS can support. In contrast we focus on  $f$ -DP, which captures enough information to reconstruct any divergence by post-processing (Proposition B.1. in Dong et al. (2019)). Our main objective is different: we leverage  $f$ -DP *composition* properties to enable multi-step deep learning architectures that adapt to the input at test time with robustness guarantees.

## 2.2 Randomized Smoothing from $f$ -DP

We reconnect RS with DP, using  $f$ -DP to yield results as strong as that of Equation (1). We start with a general robustness result on  $f$ -DP classifiers, which we later build on for our main result.

**Proposition 2.1** ( *$f$ -DP Robustness*). *Let  $\mathcal{M} : \mathcal{X} \rightarrow \mathcal{Y}$  be  $f$ -DP for  $B_p(r)$  neighbourhoods, and let  $M_S : \mathcal{X} \rightarrow \arg \max_{y \in \mathcal{Y}} \mathbb{P}(\mathcal{M}(X) = y)$  be the associated smoothed classifier. Let  $y_+ \triangleq M_S(X)$  be the prediction on input  $X$ , and let  $\underline{p}_+, \overline{p}_- \in [0, 1]$  be such that  $\mathbb{P}(\mathcal{M}(X) = y_+) \geq \underline{p}_+ \geq \overline{p}_- \geq \max_{y_- \neq y_+} \mathbb{P}(\mathcal{M}(X) = y_-)$ . Then:*

$$f(1 - \underline{p}_+) \geq 1 - f(\overline{p}_-) \Rightarrow \forall e \in B_p(r), M_S(X + e) = y_+$$

*Proof.* See Appendix B1. □

Let us now instantiate Proposition 2.1 for Gaussian RS (see §2.1):

**Corollary 2.2** (RS from  $f$ -DP). *Let  $\mathcal{M} : X \rightarrow g(X + z)$ ,  $z \sim \mathcal{N}(0, \sigma^2 \mathbb{I}^d)$ , and  $M_S : X \rightarrow \arg \max_{y \in \mathcal{Y}} \mathbb{P}(\mathcal{M}(X) = y)$  be the associated smooth model. Let  $y_+ \triangleq M_S(X)$  be the prediction on input  $X$ , and let  $\underline{p}_+, \bar{p}_- \in [0, 1]$  be such that  $\mathbb{P}(\mathcal{M}(X) = y_+) \geq \underline{p}_+ \geq \bar{p}_- \geq \max_{y_- \neq y_+} \mathbb{P}(\mathcal{M}(X) = y_-)$ . Then  $\forall e \in B_2(r_x)$ ,  $M_S(X + e) = y_+$ , with:*

$$r_X = \frac{\sigma}{2} (\Phi^{-1}(\underline{p}_+) - \Phi^{-1}(\bar{p}_-)).$$

*Proof.* See Appendix B2. *Sketch:*  $\mathcal{M}$  is a Gaussian mechanism, and is  $G_{\frac{\sigma}{r}}$ -DP for any  $r$  ( $B_2(r)$  neighbourhood). We apply Proposition 2.1 and maximize  $r$  such that  $G_{\frac{\sigma}{r}}(1 - \underline{p}_+) \geq 1 - G_{\frac{\sigma}{r}}(\bar{p}_-)$ .  $\square$

### 2.3 Adaptive Randomized Smoothing

While Proposition 2.1 is new, so far we have only used it to reprove the known result of Corollary 2.2. So why is this connection between  $f$ -DP and robustness useful? Our key insight is that we can leverage adaptive composition results at the core of DP algorithms to *certify multi-step methods that adapt to their inputs at test time*. Such adaptive defences have seen recent empirical interest, but either lack formal guarantees, or provide only limited adaptivity in practice (§5). For the first time we derive a *sound and high-dimensional* adaptive method for certification.

We formalize adaptive multi-step certification as follows. Consider  $k$  randomized Gaussian mechanisms  $\mathcal{M}_1, \dots, \mathcal{M}_k$  (our adaptive steps), such that  $m_i \sim \mathcal{M}_i(X | m_{<i})$ , and for all  $r \geq 0$  we have that  $\mathcal{M}_i$  is  $G_{r/\sigma_i}$ -DP for the  $B_2(r)$  neighbouring definition. Note that the computation  $\mathcal{M}_i$  can depend on previous results, as long as it is  $G_{r/\sigma_i}$ -DP. Further consider a (potentially randomized) post-processing classifier  $g(m_1, \dots, m_k) = y \in \mathcal{Y}$ .

**Theorem 2.3 (Main result: Adaptive RS).** *Using definitions above, let  $\mathcal{M} : X \rightarrow g(m_1, \dots, m_k) \in \mathcal{Y}$ ,  $(m_1, \dots, m_k) \sim (\mathcal{M}_1(X), \dots, \mathcal{M}_k(X | m_{<k}))$ , and the associated smoothed model be  $M_S : X \rightarrow \arg \max_{m \in \mathcal{Y}} \mathbb{P}(\mathcal{M}(X) = y)$ . Let  $y_+ \triangleq M_S(X)$  be the prediction on input  $X$ , and let  $\underline{p}_+, \bar{p}_- \in [0, 1]$  be such that  $\mathbb{P}(\mathcal{M}(X) = y_+) \geq \underline{p}_+ \geq \bar{p}_- \geq \max_{y_- \neq y_+} \mathbb{P}(\mathcal{M}(X) = y_-)$ . Then  $\forall e \in B_2(r_x)$ ,  $M_S(X + e) = y_+$ , with:*

$$r_X = \frac{1}{2 \sqrt{\sum_{i=1}^k \frac{1}{\sigma_i^2}}} (\Phi^{-1}(\underline{p}_+) - \Phi^{-1}(\bar{p}_-)).$$

*Proof.* By adaptive composition of Gaussian DP mechanisms (Equation (3)),  $\mathcal{M}$  is  $G_{\mu}$ -DP with  $\mu = \sqrt{\sum_{i=1}^k \frac{r^2}{\sigma_i^2}} = r \sqrt{\sum_{i=1}^k \frac{1}{\sigma_i^2}}$ . We can then apply Corollary 2.2 with  $\sigma = 1/\sqrt{\sum_{i=1}^k \frac{1}{\sigma_i^2}}$ .  $\square$

We focus on Gaussian RS, but a similar argument applies to general  $f$ -DP mechanisms for which we can compute  $f_i$  at any  $r$ , and the composition  $f_i \otimes \dots \otimes f_k$ , potentially using numerical techniques such as that of Gopi et al. (2021). For Gaussian noise, Theorem 2.3 leverages strong results from DP to provide a perhaps surprising result: there is no cost to adaptivity, in the sense that  $k$  independent measurements of input  $X$  with Gaussian noise (without adaptivity) of respective variance  $\sigma_i^2$  can be averaged to one measurement of variance  $\sigma^2 = 1/\sum_{i=1}^k \sigma_i^{-2}$ . To show this, we can use a weighted average to minimize variance (see e.g., Equation 4 in Honaker (2015)), with  $c_j = \sigma_j^{-2}/\sum_{i=1}^k \sigma_i^{-2}$  yielding  $\sigma^2 = \sum_{j=1}^k c_j^2 \sigma_j^2 = \sum_{j=1}^k \sigma_j^{-2}/(\sum_{i=1}^k \sigma_i^{-2})^2 = 1/\sum_{i=1}^k \sigma_i^{-2}$ . The ARS  $r_X$  from Theorem 2.3 is identical to that of one step RS from Corollary 2.2 using this variance: *adaptivity over multi-step computation comes with no decrease in certified radius*.

### 2.4 ARS against $L_\infty$ -Bounded Adversaries

How can we leverage the multi-step adaptivity from Theorem 2.3 to increase certified accuracy? We focus on two-step certified defence against  $L_\infty$ -bounded attacks to increase accuracy by adaptivity. Previous work already notes that RS applies to  $L_\infty$ -bounded attackers (Lécuyer et al., 2019; Cohen

et al., 2019), using the fact that  $\forall X \in \mathbb{R}^d, \|X\|_2 \leq \sqrt{d}\|X\|_\infty$ , and hence that  $X - X' \in B_\infty(r^\infty) \Rightarrow X - X' \in B_2(\sqrt{d} \cdot r^\infty)$ . Using Corollary 2.2, this yields:

$$r_X^\infty = \frac{\sigma}{2\sqrt{d}}(\Phi^{-1}(\underline{p}_+) - \Phi^{-1}(\overline{p}_-)). \quad (4)$$

While  $L_\infty$ -specific RS theory exists (Yang et al., 2020), further work by Blum et al. (2020) has found that Gaussian RS performs advantageously in practice. However, Blum et al. (2020); Kumar et al. (2020); Wu et al. (2021) show that the  $\sqrt{d}$  dependency cannot be avoided for a large family of distributions, leading the authors to speculate that RS might be inherently limited for  $L_\infty$  certification of predictions on high dimensional images. To side-step this issue, we use two-steps adaptivity to first select subsets of the image important to the classification task (thereby reducing dimension), and then make the prediction based on the selected subset. Formally:

**Proposition 2.4** (Adaptive RS for  $L_\infty$ ). *Define the following pair of (adaptive) mechanisms:*

$$\mathcal{M}_1 : X \rightarrow X + z_1 \triangleq m_1, \quad z_1 \sim \mathcal{N}(0, \sigma_1^2 \mathbb{I}^d) \quad (5)$$

Then, with any function  $w : \mathbb{R}^d \rightarrow [0, 1]^d$  (interpreted as a mask):

$$\mathcal{M}_2 : (X, m_1) \rightarrow w(m_1) \odot X + z_2 \triangleq m_2, \quad z_2 \sim \mathcal{N}(0, \frac{\|w(m_1)\|_2^2}{d} \sigma_2^2 \mathbb{I}^d) \quad (6)$$

where  $\odot$  is the element-wise product; and the final prediction function  $g : m_1, m_2 \rightarrow \mathcal{Y}$ .

Consider the mechanism  $\mathcal{M}$  that samples  $m_1 \sim \mathcal{M}_1$ , then  $m_2 \sim \mathcal{M}_2$ , and finally outputs  $g(m_1, m_2)$ ; and the associated smoothed classifier  $M_S : X \rightarrow \arg \max_{y \in \mathcal{Y}} \mathbb{P}(\mathcal{M}(X) = y)$ . Let  $y_+ \triangleq M_S(X)$  be the prediction on input  $X$ , and let  $\underline{p}_+, \overline{p}_- \in [0, 1]$  be such that  $\mathbb{P}(\mathcal{M}(X) = y_+) \geq \underline{p}_+ \geq \overline{p}_- \geq \max_{y_- \neq y_+} \mathbb{P}(\mathcal{M}(X) = y_-)$ . Then  $\forall e \in B_\infty(r_X^\infty)$ ,  $M_S(X + e) = y_+$ , with:

$$r_X^\infty = \frac{1}{2\sqrt{d(\frac{1}{\sigma_1^2} + \frac{1}{\sigma_2^2})}}(\Phi^{-1}(\underline{p}_+) - \Phi^{-1}(\overline{p}_-)). \quad (7)$$

*Proof.* Consider any  $X, X'$  s.t.  $X - X' \in B_\infty(r^\infty)$ . We analyze  $\mathcal{M}_1$  and  $\mathcal{M}_2$  in turn.  $\|X - X'\|_2 \leq \sqrt{d}\|X - X'\|_\infty$ , so  $X - X' \in B_2(\sqrt{d}r^\infty)$ , and  $\mathcal{M}_1$  is  $G_{\mu_1}$ -DP with  $\mu_1 = \frac{r^\infty \sqrt{d}}{\sigma_1}$ .

$\|w(m_1) \odot X - w(m_1) \odot X'\|_2 = \|w(y_1) \odot (X - X')\|_2 \leq \|w(y_1)\|_2 \|X - X'\|_\infty$  so  $X - X' \in B_2(\|w(y_1)\|_2 r^\infty)$  and  $\mathcal{M}_2$  is  $G_{\mu_2}$ -DP with  $\mu_2 = \frac{\|w(y_1)\|_2 r^\infty}{\|w(y_1)\|_2 \sigma_2 / \sqrt{d}} = \frac{r^\infty \sqrt{d}}{\sigma_2}$ .

Applying Theorem 2.3 with  $\sqrt{\frac{(r^\infty)^2 d}{\sigma_1^2} + \frac{(r^\infty)^2 d}{\sigma_2^2}} = r^\infty \sqrt{d(\frac{1}{\sigma_1^2} + \frac{1}{\sigma_2^2})}$  concludes the proof.  $\square$

**Important remarks. 1.**  $w(\cdot)$  is a masking function, adaptively reducing (if  $w_i(m_1) \ll 1$ ) the value of  $X_i$  and thereby the attack surface of an  $L_\infty$  attacker. This reduces the effective dimension of the input to  $\mathcal{M}_2$ . **2.** Reducing the dimension enables a reduction in the noise variance in  $\mathcal{M}_2$ , at fixed privacy guarantee  $G_{\mu_2}$ . The variance reduction is enabled for all dimensions in the input, even those that are not masked ( $w_i(m_1) \approx 1$ ). As a result, the variance of the noise in  $\mathcal{M}_2$  scales as  $\|w(m_1)\|_2^2 \leq d$ . The more masking, the lower the variance. It may help to consider the change of variables  $\sigma \leftarrow \sigma/\sqrt{d}$  in Equation (4), and  $\sigma_{1,2} \leftarrow \sigma_{1,2}/\sqrt{d}$  in Proposition 2.4, to remove  $d$  from  $r_X^\infty$  and scale the noise variance with  $d$ . For RS (Equation (4)), the noise variance scales as  $d$ . For ARS, only Equation (5) (the first step) suffers from variance scaled by  $d$ , while the second step's variance (Equation (6)) scales as  $\|w(m_1)\|_2^2$ , which can be much smaller than  $d$  when a large part of the image is masked. Reduced variance translates into higher accuracy, as well as  $\underline{p}_+$  and  $\overline{p}_-$  being further apart, for a larger  $r_X^\infty$ . **3.** The variance reduction due to masking applies in the translation from the  $B_\infty(r^\infty)$  bound on the attack to the  $B_2(r)$  sensitivity used in ARS. This variance reduction would not apply to an  $L_2$ -bounded adversary. Hence, our two-steps ARS architecture for  $L_\infty$ -bounded adversaries does not reduce to bounding  $L_\infty$  with  $L_2$  as the traditional RS application does, and our gains come explicitly from variance reduction enabled by adaptive masking.

### 3 Two-Step ARS for $L_\infty$ Certification of Image Classification

Figure 1 shows our deep learning architecture based on Proposition 2.4. The first step,  $\mathcal{M}_1$ , adds noise to input  $X$  and post-processes the result into a mask  $w(m_1)$ . The second step,  $\mathcal{M}_2$ , takes masked input  $w(m_1) \odot X$  and adds noise. Finally, the base classifier  $g$  post-processes a weighted average of  $m_1, m_2$  to output a label. The whole model is trained end-to-end on the classification task. In RS, only the path going through  $\mathcal{M}_2$  is present. This is equivalent to setting  $\sigma_2 = \sigma$  and  $w(\cdot) = 1$ , with no  $\mathcal{M}_1$ . In both cases, the final predictions are averaged over the noise to create the smoothed classifier. The ARS architecture introduces several new components, which we next describe.

**Budget Splitting:** the noise budget  $\sigma$  (Figure 1; red) is split to assign noise levels to the two steps  $\mathcal{M}_1$  and  $\mathcal{M}_2$ . We parameterize ARS with the same  $\sigma$  as standard RS then split it by the  $f$ -DP composition formula from Equation (3). In practice, we assign  $\sigma_1 \geq \sigma$  to  $\mathcal{M}_1$ , and then  $\sigma_2 = 1/\sqrt{\frac{1}{\sigma_2^2} - \frac{1}{\sigma_1^2}}$ . We set  $\sigma_1$  by either fixing it to a constant or learning it end-to-end.

**Masking:** the mask model  $w(\cdot)$  takes the noisy image from  $\mathcal{M}_1$  and predicts a weighting (one value in  $[0, 1]$  per input pixel) that is multiplied with the input element-wise (denoted  $\odot$  in Proposition 2.4). The model is a U-Net architecture, which makes pixel-wise predictions, and acts as a post-processing of  $\mathcal{M}_1$  in the  $f$ -DP analysis. Our masking enables test-time adaptivity to reduce the noise variance for  $\mathcal{M}_2$ , via the mask’s dependence on the input through  $m_1$ .

**Mechanism output averaging:** to fully leverage both steps’ information, we take a weighted average of the outputs  $m_1$  and  $m_2$  before passing the result to the base classifier  $g$ . For a particular input pixel  $i$ , denote  $X_i$  the value of pixel,  $w_i \in [0, 1]$  its mask weight (we omit the explicit dependency on  $m_1$  in  $w$  for compactness), and  $m_{1,i}, m_{2,i}$  the respective values output by  $\mathcal{M}_1$  and  $\mathcal{M}_2$ . Then, the final value of pixel  $i$  in the averaged input will be  $\hat{X}_i \triangleq c_{1,i}m_{1,i} + c_{2,i}m_{2,i}$ .

We set  $c_{1,i}, c_{2,i}$  such that  $\hat{X}_i$  is the unbiased estimate of  $X_i$  with smallest variance. First, we set  $c_{1,i} + w_i c_{2,i} = 1$ , such that  $\mathbb{E}[\hat{X}_i] = c_{1,i}X_i + c_{2,i}w_i X_i = X_i$ . Second, we minimize the variance. Notice that  $\mathbb{V}[\hat{X}_i] = c_{1,i}^2\sigma_1^2 + c_{2,i}^2\|w\|_2^2\sigma_2^2 = (1 - w_i c_{2,i})^2\sigma_1^2 + c_{2,i}^2\|w\|_2^2\sigma_2^2$ : this is a convex function in  $c_{2,i}$  minimized when its gradient in  $c_{2,i}$  is zero. Plugging back into the constraint to get  $c_{1,i}$ , we obtain the following weights:  $c_{1,i} = \frac{\|w\|_2^2\sigma_2^2}{\sigma_1^2 w_i^2 + \|w\|_2^2\sigma_2^2}$ , and  $c_{2,i} = \frac{\sigma_1^2 w_i}{\sigma_1^2 w_i^2 + \|w\|_2^2\sigma_2^2}$ .

The averaged noisy input  $\hat{X}$  is finally fed to the base classifier  $g$  for prediction. The smoothed classifier  $M_S$  averages predictions (over noise draws) over the entire pipeline. The parameters of  $w$  and  $g$  (and  $\sigma_1$  if not fixed) are learned during training and are fixed at inference/certification time.

## 4 Experiments

We evaluate on certified  $L_\infty$  and standard test accuracy. Certified accuracy at radius  $r^\infty$  is the percentage of test samples that are correctly classified **and** have an  $L_\infty$  certificate radius  $r_X^\infty \geq r^\infty$ . Standard accuracy is obtained for  $r^\infty = 0$ .

**Datasets** We evaluate on CIFAR-10 (Krizhevsky, 2009) in §4.1, CelebA (Liu et al., 2015) (specifically the unaligned HD-CelebA-Cropper edition) in §4.2, and ImageNet (Deng et al., 2009) in §4.3. We measure adaptivity on CIFAR-10 and CelebA by designing challenging benchmarks requiring adaptivity, and measure scalability on ImageNet.

**Models** We choose the standard ResNet (He et al., 2016) models as base classifiers  $g$  with ResNet-110 for CIFAR-10 and ResNet-50 for CelebA and ImageNet. For ARS, our mask model  $w$  is a simplified U-Net (Ronneberger et al., 2015) (see Appendix C for details). For the noise budget, we find that a fixed budget split performs reliably, and so in all experiments we split by  $\sigma_1 = \sigma_2 = \sqrt{2}\sigma$ .

**Methods** We compare to standard and strong static methods, design a baseline specifically for our masking approach, and evaluate the only sound input-dependent method prior to ARS. Cohen et al. is the standard approach to RS (Cohen et al., 2019). UniCR (Hong et al., 2022) learns the noise distribution for RS during training but is static during testing (while they propose an adaptive variant, it is not sound, so we restrict our comparison to the training variant). We tune hyper-parameters, and perform a grid search for  $\beta$  (the parameter of the noise distribution) to maximize certified accuracy. We find  $\beta = 2.25$  (close to a Gaussian, with smaller tails) to perform best. *Static Mask* is our baseline

Setting/Approach	Cohen et al.	Static Mask	UniCR	Súkeník et al. <sup>Δ</sup>	ARS <sup>Δ</sup>
$\sigma = 0.75, k = 32$	55.5 (0.8)	<b>57.8 (0.8)</b>	50.9 (5.9)	49.8 (1.0)	57.3 (0.6)
$\sigma = 0.75, k = 40$	52.1 (0.4)	57 (0.7)	44.3 (1.2)	48.1 (1.6)	<b>58.1 (1.8)</b>
$\sigma = 0.75, k = 48$	52.5 (1.2)	56 (0.8)	49.0 (2.2)	43.1 (3.1)	<b>57.6 (1.5)</b>
$\sigma = 0.75, k = 64$	49.4 (2.0)	51.6 (1.0)	-	-	<b>56.5 (2.6)</b>
$\sigma = 0.12, k = 48$	80.1 (0.8)	80.9 (0.7)	76.3 (1.9)	76.1 (4.1)	<b>83.6 (0.4)</b>
$\sigma = 0.5, k = 48$	64.3 (0.2)	64.1 (1.6)	54.0 (2.2)	55.9 (1.4)	<b>66.0 (0.8)</b>
$\sigma = 1.5, k = 48$	30.8 (0.2)	<b>34.9 (2.4)</b>	30.7 (0.9)	26.5 (0.7)	34.3 (0.2)
$\sigma = 0.12, k = 64$	80.9 (1.0)	81.3 (1.0)	-	-	<b>82.3 (1.0)</b>
$\sigma = 0.5, k = 64$	61.6 (2.7)	64 (1.4)	-	-	<b>65.4 (1.8)</b>
$\sigma = 1.5, k = 64$	28.3 (0.2)	25.9 (3.2)	-	-	<b>30.6 (1.0)</b>

Table 1: **Standard Accuracy** ( $r = 0$ ) on **CIFAR-10 (20kBG)**. Our 20kBG benchmark places CIFAR-10 images on larger background images. We report the mean accuracy and standard deviation over three seeds. ARS achieves higher accuracy across noise  $\sigma$  and input dimension  $k$ . <sup>Δ</sup> indicates adaptivity.

that learns a fixed mask during training that does not adapt during testing. The mask is directly parameterized as pixel-wise weights that we multiply with the input and optimize jointly with the base classifier. Relative to ARS in Figure 1, this removes  $\mathcal{M}_1$ , sets  $\sigma_2 = \sigma$ , and makes  $w(\cdot) = W$  static parameters rather than an adaptive prediction. Súkeník et al. (2021) conditions the variance  $\sigma$  for RS on the input and is therefore test-time adaptive. We use code provided by the authors as is. Comparing ARS to the static baselines measures the value of test-time adaptivity, and comparing ARS to the variance adaptivity of Súkeník et al. measures the importance of more high-dimensional and expressive adaptation.

#### 4.1 CIFAR-10 Benchmark: Classification with Distractor Backgrounds

Input dimension is a key challenge in  $L_\infty$  certification using RS (see §2.4). We design our 20kBG benchmark to vary this parameter without affecting the task: we superimpose CIFAR-10 images onto a larger background from the 20k background images dataset Li et al. (2022a), split them into train and test sets, and resize to  $k \times k$  pixels. The CIFAR-10 image is placed at random along the edges of the background image to maximize spatial variation. The spurious background increases the dimension of the input ( $= k \times k \times 3$ ), making  $L_\infty$  certification with RS more challenging, but it is uninformative for the task of CIFAR-10 by construction. Our mask model ( $\mathcal{M}_1$ ) needs to learn to ignore the background to reduce the effective dimension of the input.

Table 1 summarizes the standard accuracy ( $r = 0$ ) of each approach on the different settings. In the top section, we vary  $k$  (i.e. dimensionality) in  $\{32, 48, 64\}$ , where  $k = 32$  corresponds to original CIFAR-10 images. We keep  $\sigma$  fixed to 0.75 across these experiments. In next two rows, we vary  $\sigma \in \{0.12, 0.5, 1.5\}$  at fixed  $k = 48$  and  $k = 64$ , respectively. Figure 2 shows the certified test accuracy at different radii  $r^\infty$  for ARS and all baselines we consider.

We make three observations. First, in most cases ARS outperforms all the baselines (static mask is slightly better with no distractor background, and with very high  $\sigma$  when all methods have low accuracy) reaching a standard accuracy 4.9 percentage points higher than the best baseline on our main setup ( $k = 64, \sigma = 0.75$ ). Hong et al. (2022) and our own static mask baselines are the best performing, but all are close to Cohen et al. (2019) as these approaches provide little adaptivity. The improved standard accuracy of ARS translates to an improved certified accuracy at all certification levels (again except without distractor backgrounds, and with very high  $\sigma$  when all methods have low accuracy). This is because ARS makes more accurate and confident predictions on more test examples, leading to a larger radius.

Second, as we grow the input dimension ( $k$ ), the accuracy of ARS remains stable whereas that of baselines goes down, resulting in an increasing gap. For  $k = 32$  the best baseline (static mask) beats ARS by 0.5 percentage points, whereas the gap between the same approaches reaches 1.6 percentage points in favor of ARS when  $k = 48$ , and 4.9 points at  $k = 64$ . This is because ARS’ mask is able to rule out spurious background information, reducing the noise in the second step, as shown on Figure 3. Thanks to this masking, ARS is much less sensitive to increases in dimensionality (see Table 1).

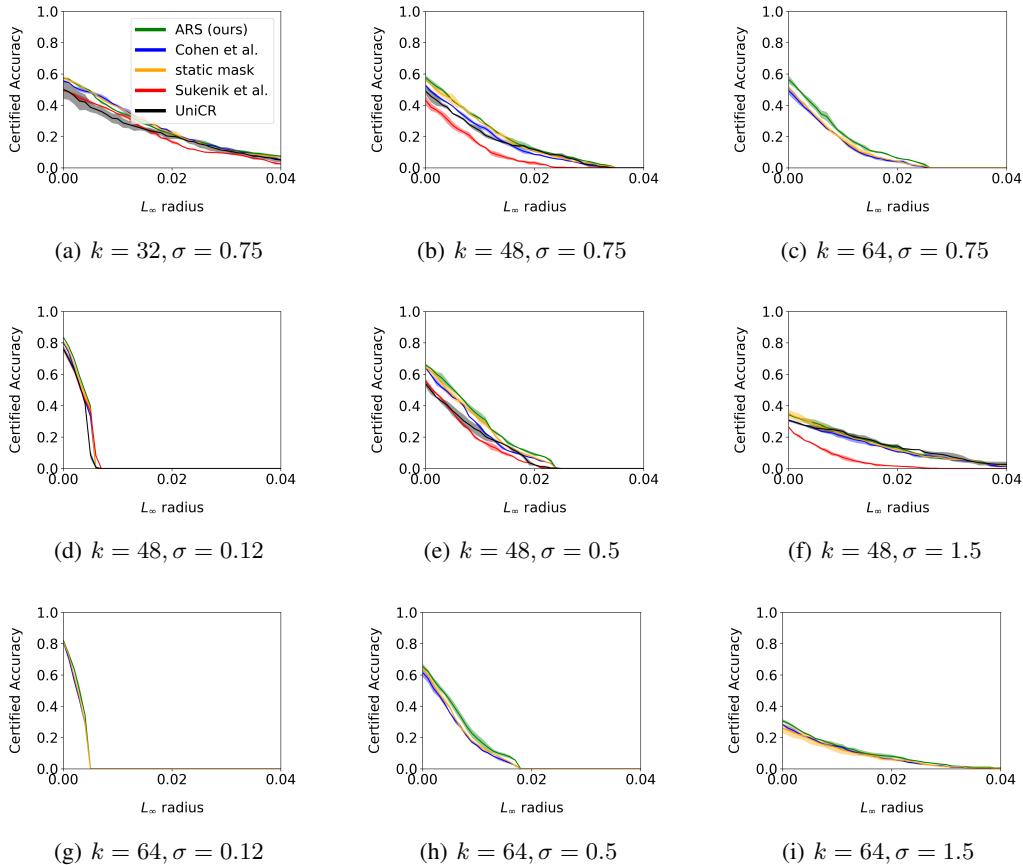


Figure 2: **Certified Test Accuracy on CIFAR-10 (20kB)**. (a)-(c) show the effect of dimensionality for (a) no background /  $k = 32$ , (b)  $k = 48$ , and (c)  $k = 64$  for constant  $\sigma = 0.75$ . (d)-(f) show the effect of noise for (d)  $\sigma = 0.12$ , (e)  $\sigma = 0.5$  and (f)  $\sigma = 1.5$  with dimensionality fixed to  $k = 48$ . (g)-(i) show the effect of noise for (d)  $\sigma = 0.12$ , (e)  $\sigma = 0.5$  and (f)  $\sigma = 1.5$  with dimensionality fixed to  $k = 64$ . These results are in our 20kB setting where a CIFAR-10 image is placed randomly along the edges of a background image. Each line is the mean and the shaded interval covers  $\pm 1$  standard deviation across seeds.

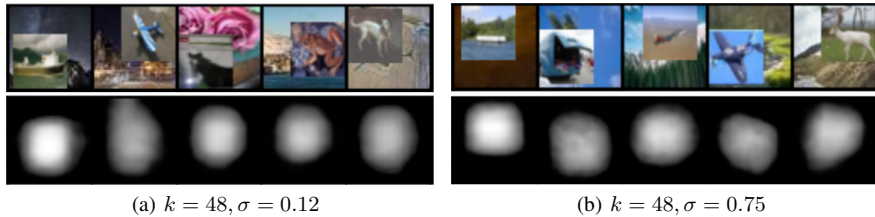


Figure 3: **ARS Masks on CIFAR-10 (20kB)** select the task-relevant input over the distractor background.

Third, we observe that ARS does much better than the baselines in low to moderate noise regimes ( $\sigma = 0.5, 0.75$ ) whereas it performs similarly or even slightly worse in high noise regimes ( $\sigma = 1.5$ ). This is because in the high noise regime, the first ARS step is too noisy for the mask to be efficient.

ARS training and inference requires additional computation. To certify a single input ( $k = 32$ ), Cohen et al. (2019) takes  $\sim 12$  seconds while ARS takes  $\sim 26$  seconds (as measured on an NVIDIA A100 80Gb GPU). This  $2\times$  overhead does however yield improved certified accuracy.

## 4.2 CelebA Benchmark: Classification Without Spatial Alignment

To evaluate ARS on a more realistic task with natural spatial variation, we use the CelebA face dataset in its unaligned version. We focus on the “mouth slightly open” (label 21) binary classification task because mouth location and shape vary. Furthermore we hypothesize that the necessary input for this task is well-localized, which affords an opportunity for the masking model to reduce the



Setting/Approach	Cohen et al.	Static Mask	ARS
CelebA, $\sigma = 0.12$	94.7 (0.5)	95.7 (1.2)	<b>96.3(0.9)</b>
CelebA, $\sigma = 0.75$	88.7 (1.2)	89.0 (1.4)	<b>92.3(0.9)</b>
CelebA, $\sigma = 1.5$	77.7 (2.5)	74.3 (1.7)	<b>81.0(2.2)</b>

Table 2: **Standard test accuracy ( $r = 0$ ) on CelebA (unaligned and cropped)**. ARS is equal or better. Adaptivity handles the higher spatial dimensions ( $160 \times 160$ ) and variation of these inputs.

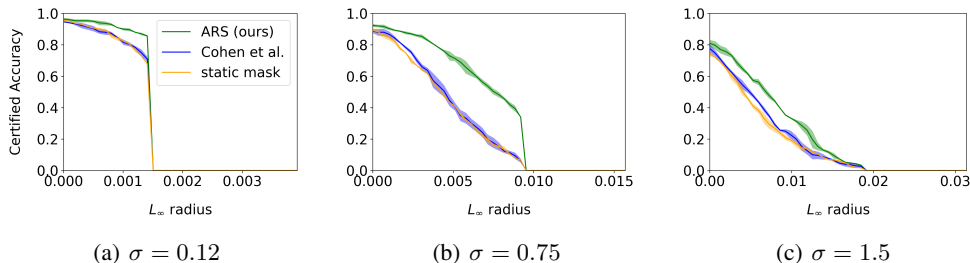


Figure 4: **Certified test accuracy on CelebA (unaligned and cropped)**. We evaluate static methods and ARS to measure the value of adaptivity. Each line is the mean and the shading covers  $\pm 1$  standard deviation across three seeds. Adaptivity helps at all noise levels (note the varying x-axis to compensate for noise level).

effective input dimension. The dataset consists of images with varied resolution, and meta-data about the position of different features, including the mouth. To make a more challenging benchmark we randomly crop all images to  $160 \times 160$  pixels for more spatial variation. The only crop constraint is that the mouth is  $\geq 10$  pixels from the edge to ensure sufficient input to solve the task. Figure 5 shows example images from the test set, their respective masks from ARS, and the baseline static mask.

Figure 4 shows the certified accuracy for ARS, Cohen et al. (2019), and static mask, for three levels of the noise  $\sigma$ . First, both baselines perform very similarly. We can see from Figure 5 that the static mask is approximately identity (notice the  $\geq 0.99$  scale), with only very slight dimming on the edges. This is because the mouth is not centred in our benchmark, so there is no one-size-fits-all mask. Second, ARS is able to predict a sparse mask that focuses on areas likely to have the mouth. The mask adapts to each input at test time, which is what enables the sparsity without performance degradation. Third, this sparse mask leads to a large noise reduction, enabling ARS to drastically improve both standard and certified accuracy. For instance, with  $\sigma = 0.75$ , ARS improves the accuracy from 88.7% to 92.3% (a 3.6 points improvement), while the certified accuracy at  $r^\infty = 0.005$  jumps from 40.7% to 71.3% (a more than 30 points improvement!). At lower noise ( $\sigma = 0.12$ ) there is no increase in accuracy, but certified accuracy increases from 81.7% to 90.0% at  $r^\infty = 0.001$ . At larger noise ( $\sigma = 1.5$ ), the static mask struggles to perform as well, but ARS sees significant increases (10 percentage points in accuracy, and 20.0% to 31.3% in certified accuracy at  $r^\infty = 0.01$ ).



Figure 5: ARS masks are localized and input specific.

### 4.3 ImageNet Benchmark: Classification on the Standard Large-Scale Dataset

To evaluate the scalability of ARS we experiment on ImageNet with  $\sigma = 0.5$  (without any modification). We compare with Cohen et al. (2019), which we reproduce for this large-scale setting. We also compare with static mask, and random mask (our mask model randomly initialized without training) to evaluate the effect of blind masking. We evaluate two versions of ARS: our regular model, trained end-to-end; and a version in which we fix the base classifier to that of Cohen et al. (2019) and only train our mask model for 10 epochs (with the Adam optimizer and constant learning rate). Figure 6 shows the certified accuracy for all models. We make three observations. First,

by only training a mask model ARS is able to improve results by 1 percentage point (from 57% to 58%). Certified accuracy remains close to that of [Cohen et al. \(2019\)](#) at all radius, but ARS can certify slightly larger radius: At  $r^\infty = 0.005$ , the certified accuracy of [Cohen et al. \(2019\)](#), static mask, and random mask are 0, while that of ARS is still 15% (which drops to 0 shortly after). Second, ARS trained end-to-end reaches an accuracy of 60%, 3 points higher than that of [Cohen et al. \(2019\)](#). The certified accuracy is higher by similar margins up to  $r^\infty = 0.003$ , where it becomes a bit lower than that of [Cohen et al. \(2019\)](#), before again certifying a slightly better maximum radius, with 13% accuracy at  $r^\infty = 0.005$ . Third, a randomly initialized mask model yields an accuracy of 49% showing that our ARS model benefits are not explained by random masking, which is consistent with the mask learning to reduce the input dimension while preserving input semantics important to the task. Overall, these results show that ARS is general in that its adaptivity does not over-specialize to our adaptation benchmarks, and that it can scale to large datasets and complex classification tasks.

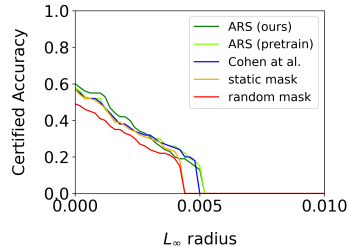


Figure 6: ImageNet  $\sigma = 0.5$ .

## 5 Discussion

**Limitations:** The multi-step adaptivity of ARS improves certification at the cost of increased model size and computation for RS. This impacts both training and testing computation, and is especially costly in the context of RS due to the Monte-Carlo estimation of the model’s expected predictions (over several forward passes at inference time). While we empirically show improvement by ARS, it would be interesting and important to investigate how it combines with other RS improvements such as adversarial training ([Salman et al., 2019](#)), consistency regularization ([Jeong and Shin, 2020](#)), higher order certification ([Mohapatra et al., 2020](#)), double sampling ([Li et al., 2022b](#)), and denoising by diffusion ([Carlini et al., 2022](#)).

**Implications:** revisiting heuristic adaptive defences (as surveyed in [Croce et al. \(2022\)](#)) through the lens of ARS could help improve the empirical performance of provable defences. ARS may require extensions, but could eventually enable the formal analysis of input purification (e.g., [Song and Kim \(2018\)](#); [Nie et al. \(2022\)](#); [Yoon et al. \(2021\)](#)), or leverage DP-SGD ([Abadi et al., 2016](#)) to analyze defences that update by test-time optimization ([Alfarra et al., 2022b](#); [Hwang et al., 2022](#); [Mao et al., 2021](#)). Going further, one could leverage the vast DP literature to extend ARS, enabling fully-adaptive variance defences inspired by [Alfarra et al. \(2022a\)](#) by leveraging privacy odometers ([Rogers et al., 2016](#); [Lécuyer, 2021](#); [Whitehouse et al., 2023](#)).

To conclude: we introduced Adaptive Randomized Smoothing (ARS) to reconnect RS with DP theory, to propose a new two-step defence for deep image classification, and to rigorously analyze such adaptive defences that condition on inputs at test time. This framework opens promising avenues for designing ML models that are adaptively and soundly robust with provable guarantees about their updates on natural and adversarial inputs.

## References

Martin Abadi, Andy Chu, Ian Goodfellow, H Brendan McMahan, Ilya Mironov, Kunal Talwar, and Li Zhang. Deep learning with differential privacy. In *Proceedings of the 2016 ACM SIGSAC conference on computer and communications security*, 2016.

Motasesm Alfarra, Adel Bibi, Philip HS Torr, and Bernard Ghanem. Data dependent randomized smoothing. In *Uncertainty in Artificial Intelligence*, pages 64–74. PMLR, 2022a.

Motasesm Alfarra, Juan C. Perez, Ali Thabet, Adel Bibi, Philip H.S. Torr, and Bernard Ghanem. Combating adversaries with anti-adversaries. *Proceedings of the AAAI Conference on Artificial Intelligence*, 2022b.

Anish Athalye, Nicholas Carlini, and David Wagner. Obfuscated gradients give a false sense of security: Circumventing defenses to adversarial examples. In *International conference on machine learning*, 2018.

- Avrim Blum, Travis Dick, Naren Manoj, and Hongyang Zhang. Random smoothing might be unable to certify  $\ell_\infty$  robustness for high-dimensional images. *The Journal of Machine Learning Research*, 2020.
- Yulong Cao, Ningfei Wang, Chaowei Xiao, Dawei Yang, Jin Fang, Ruigang Yang, Qi Alfred Chen, Mingyan Liu, and Bo Li. Invisible for both camera and lidar: Security of multi-sensor fusion based perception in autonomous driving under physical-world attacks. In *2021 IEEE Symposium on Security and Privacy (SP)*, 2021.
- Nicholas Carlini, Florian Tramer, Krishnamurthy Dj Dvijotham, Leslie Rice, Mingjie Sun, and J Zico Kolter. (certified!!) adversarial robustness for free! In *The Eleventh International Conference on Learning Representations*, 2022.
- Anirban Chakraborty, Manaar Alam, Vishal Dey, Anupam Chattopadhyay, and Debdeep Mukhopadhyay. Adversarial attacks and defences: A survey. *arXiv preprint arXiv:1810.00069*, 2018.
- Jeremy Cohen, Elan Rosenfeld, and Zico Kolter. Certified adversarial robustness via randomized smoothing. In *international conference on machine learning*, pages 1310–1320. PMLR, 2019.
- Joana C Costa, Tiago Roxo, Hugo Proença, and Pedro RM Inácio. How deep learning sees the world: A survey on adversarial attacks & defenses. *arXiv preprint arXiv:2305.10862*, 2023.
- Francesco Croce, Sven Gowal, Thomas Brunner, Evan Shelhamer, Matthias Hein, and Taylan Cemgil. Evaluating the adversarial robustness of adaptive test-time defenses. In *International Conference on Machine Learning*, pages 4421–4435. PMLR, 2022.
- Jia Deng, Wei Dong, Richard Socher, Li-Jia Li, Kai Li, and Li Fei-Fei. Imagenet: A large-scale hierarchical image database. In *2009 IEEE conference on computer vision and pattern recognition*. Ieee, 2009.
- Jinshuo Dong, Aaron Roth, and Weijie J Su. Gaussian differential privacy. *arXiv preprint arXiv:1905.02383*, 2019.
- Jinshuo Dong, Aaron Roth, and Weijie J Su. Gaussian differential privacy. *Journal of the Royal Statistical Society Series B: Statistical Methodology*, 2022.
- Krishnamurthy (Dj) Dvijotham, Jamie Hayes, Borja Balle, Zico Kolter, Chongli Qin, Andras Gyorgy, Kai Xiao, Sven Gowal, and Pushmeet Kohli. A framework for robustness certification of smoothed classifiers using f-divergences. In *International Conference on Learning Representations*, 2020. URL <https://openreview.net/forum?id=SJlKrKsFPH>.
- Sivakanth Gopi, Yin Tat Lee, and Lukas Wutschitz. Numerical composition of differential privacy. *Advances in Neural Information Processing Systems*, 2021.
- Kaiming He, Xiangyu Zhang, Shaoqing Ren, and Jian Sun. Deep residual learning for image recognition. In *Proceedings of the IEEE conference on computer vision and pattern recognition*, 2016.
- James Honaker. Efficient use of differentially private binary trees. *Theory and Practice of Differential Privacy (TPDP 2015)*, London, UK, 2015.
- Hanbin Hong, Binghui Wang, and Yuan Hong. Unicr: Universally approximated certified robustness via randomized smoothing. In *European Conference on Computer Vision*. Springer, 2022.
- Duhun Hwang, Eunjung Lee, and Wonjong Rhee. Aid-purifier: A light auxiliary network for boosting adversarial defense. In *2022 26th International Conference on Pattern Recognition (ICPR)*, 2022.
- Jongheon Jeong and Jinwoo Shin. Consistency regularization for certified robustness of smoothed classifiers. *Advances in Neural Information Processing Systems*, 2020.
- Alex Krizhevsky. Learning multiple layers of features from tiny images, 2009. URL <https://api.semanticscholar.org/CorpusID:18268744>.

- Aounon Kumar, Alexander Levine, Tom Goldstein, and Soheil Feizi. Curse of dimensionality on randomized smoothing for certifiable robustness. In *International Conference on Machine Learning*. PMLR, 2020.
- Mathias Lécuyer. Practical privacy filters and odometers with rényi differential privacy and applications to differentially private deep learning. *arXiv preprint arXiv:2103.01379*, 2021.
- Mathias Lécuyer, Vaggelis Atlidakis, Roxana Geambasu, Daniel Hsu, and Suman Jana. Certified robustness to adversarial examples with differential privacy. In *2019 IEEE symposium on security and privacy (SP)*, pages 656–672. IEEE, 2019.
- Jizhizi Li, Jing Zhang, Stephen J Maybank, and Dacheng Tao. Bridging composite and real: towards end-to-end deep image matting. *International Journal of Computer Vision*, 2022a.
- Linyi Li, Jiawei Zhang, Tao Xie, and Bo Li. Double sampling randomized smoothing. In *International Conference on Machine Learning*. PMLR, 2022b.
- Linyi Li, Tao Xie, and Bo Li. Sok: Certified robustness for deep neural networks. In *2023 IEEE symposium on security and privacy (SP)*, 2023.
- Ziwei Liu, Ping Luo, Xiaogang Wang, and Xiaoou Tang. Deep learning face attributes in the wild. In *Proceedings of International Conference on Computer Vision (ICCV)*, December 2015.
- C. Mao, M. Chiquier, H. Wang, J. Yang, and C. Vondrick. Adversarial attacks are reversible with natural supervision. In *2021 IEEE/CVF International Conference on Computer Vision (ICCV)*, 2021.
- Jeet Mohapatra, Ching-Yun Ko, Tsui-Wei Weng, Pin-Yu Chen, Sijia Liu, and Luca Daniel. Higher-order certification for randomized smoothing. *Advances in Neural Information Processing Systems*, 2020.
- Weili Nie, Brandon Guo, Yujia Huang, Chaowei Xiao, Arash Vahdat, and Animashree Anandkumar. Diffusion models for adversarial purification. In *International Conference on Machine Learning*, 2022.
- Apapan Pumsirirat and Yan Liu. Credit card fraud detection using deep learning based on auto-encoder and restricted boltzmann machine. *International Journal of advanced computer science and applications*, 2018.
- Ryan M Rogers, Aaron Roth, Jonathan Ullman, and Salil Vadhan. Privacy odometers and filters: Pay-as-you-go composition. *Advances in Neural Information Processing Systems*, 2016.
- Olaf Ronneberger, Philipp Fischer, and Thomas Brox. U-net: Convolutional networks for biomedical image segmentation. In *Medical image computing and computer-assisted intervention—MICCAI 2015: 18th international conference, Munich, Germany, October 5-9, 2015, proceedings, part III 18*. Springer, 2015.
- Hadi Salman, Jerry Li, Ilya Razenshteyn, Pengchuan Zhang, Huan Zhang, Sebastien Bubeck, and Greg Yang. Provably robust deep learning via adversarially trained smoothed classifiers. *Advances in neural information processing systems*, 2019.
- Yang Song and Taesup Kim. Sebastian nowozin stefano ermon nate kushman. pixeldefend: Leveraging generative models to understand and defend against adversarial examples. In *International Conference on Learning Representations*, 2018.
- Peter Sükénik, Aleksei Kuvshinov, and Stephan Günnemann. Intriguing properties of input-dependent randomized smoothing. *arXiv preprint arXiv:2110.05365*, 2021.
- Christian Szegedy, Wojciech Zaremba, Ilya Sutskever, Joan Bruna, Dumitru Erhan, Ian Goodfellow, and Rob Fergus. Intriguing properties of neural networks. In *International Conference on Learning Representations*, 2014. URL <http://arxiv.org/abs/1312.6199>.
- Florian Tramèr, Nicholas Carlini, Wieland Brendel, and Aleksander Madry. On adaptive attacks to adversarial example defenses. *Advances in neural information processing systems*, 33:1633–1645, 2020.

- Justin Whitehouse, Aaditya Ramdas, Ryan Rogers, and Steven Wu. Fully-adaptive composition in differential privacy. In *International Conference on Machine Learning*, 2023.
- Yihan Wu, Aleksandar Bojchevski, Aleksei Kuvshinov, and Stephan Günnemann. Completing the picture: Randomized smoothing suffers from the curse of dimensionality for a large family of distributions. In *Proceedings of The 24th International Conference on Artificial Intelligence and Statistics*, Proceedings of Machine Learning Research. PMLR, 2021. URL <https://proceedings.mlr.press/v130/wu21d.html>.
- Greg Yang, Tony Duan, J Edward Hu, Hadi Salman, Ilya Razenshteyn, and Jerry Li. Randomized smoothing of all shapes and sizes. In *International Conference on Machine Learning*. PMLR, 2020.
- Jongmin Yoon, Sung Ju Hwang, and Juho Lee. Adversarial purification with score-based generative models. In *Proceedings of the 38th International Conference on Machine Learning*, 2021.

## A $f$ -DP Background

For this background we use the DP mechanism terminology. A mechanism  $\mathcal{M}(\cdot)$  is a randomized computation taking an input and returning one sample from the distribution of outputs for this input:  $m \sim \mathcal{M}(x)$  with input  $x$  and output  $m$ . In ARS, each model step corresponds to an  $f$ -DP mechanism.

**Definitions.** Dong et al. (2019; 2022) formalize privacy as a bound on the power of hypothesis tests. Consider any two neighbouring inputs: in the most common DP applications,  $X, X'$  are two databases differing in one element; in the case of ARS against an  $L_p$  adversary,  $X, X' \in \mathbb{R}^d$  are any two inputs such that  $X - X' \in B_p(r)$ . Intuitively a randomized mechanism  $\mathcal{M}$  is private if, for any such neighbouring inputs, the distributions  $\mathcal{M}(X)$  and  $\mathcal{M}(X')$  are hard to distinguish. That is, by looking at a sample output from mechanism  $\mathcal{M}$ , it is hard to guess whether  $\mathcal{M}$  ran on  $X$  or on  $X'$ .

In  $f$ -DP (Dong et al., 2019; 2022) “hard to distinguish” is defined by a hypothesis testing problem:

$$\mathcal{H}_0 : \text{the input was } X \quad \text{vs.} \quad \mathcal{H}_1 : \text{the input was } X'.$$

The output  $m \sim \mathcal{M}$  serves as input to a rejection rule  $\phi(\cdot) \in [0, 1]$  (note: to preserve typical notations, lower-case  $\phi$  is the rejection rule, and upper-case  $\Phi$  is the standard normal CDF). The rejection rule rejects  $\mathcal{H}_0$  with probability  $\phi(m)$ , so  $\phi(m) = 0$  predicts that  $X$  was the input, and  $\phi(m) = 1$  that  $X'$  was.

Given a rejection rule  $\phi$ , we define its Type I error  $\alpha_\phi$  and type II error (or one minus the power of the rule)  $\beta_\phi$  as:

$$\alpha_\phi \triangleq \mathbb{E}_{m \sim \mathcal{M}(X)}[\phi(m)] \quad \beta_\phi \triangleq 1 - \mathbb{E}_{m \sim \mathcal{M}(X')}[\phi(m)]$$

Intuitively,  $\alpha_\phi$  is the expected amount of rejection of  $\mathcal{H}_0$  when the hypothesis is correct ( $X$  was in input, but we think  $X'$  was), also called the level of the rejection rule. On the flip side,  $\beta_\phi$  is the expected amount of non-rejection under  $\mathcal{H}_1$  ( $X'$  was in input, but we think  $X$  was).  $1 - \beta_\phi$  is called the power of the rejection rule.

For any two distributions  $\mathcal{M}(X)$  and  $\mathcal{M}(X')$ , we define the trade-off function  $T(\mathcal{M}(X), \mathcal{M}(X')) : [0, 1] \rightarrow [0, 1]$  that quantifies the minimum amount of type II error achievable at each value of type I error by any (measurable) rule; or equivalently the maximum power of any rule at each level:

$$\forall \alpha \in [0, 1], T(\mathcal{M}(X), \mathcal{M}(X'))(\alpha) = \inf_{\phi} \{\beta_\phi : \alpha_\phi \leq \alpha\}$$

Now we define  $f$ -DP: for any trade-off function  $f$ , a mechanism  $\mathcal{M}$  is  $f$ -DP if, for any neighbouring inputs  $X, X'$ ,

$$T(\mathcal{M}(X), \mathcal{M}(X')) \geq f$$

These definitions are the main technical tools we need to prove Proposition 2.1. Corollary 2.2 only adds the formula for  $f$  for the Gaussian mechanism, given in Section 2.1.

**Composition.** All other results rely on the above plus the adaptive composition of  $f$ -DP mechanisms. Such composition is key to all DP theory and algorithm design. Consider a sequence of  $N$  mechanisms  $\mathcal{M}_i$ , such that each mechanism is  $f_i$ -DP with regards to  $X, X'$ , and depends on the neighbouring input as well as the output of all previous mechanisms. More formally, under  $\mathcal{H}_0$  we have  $m_i \sim \mathcal{M}_i(X, m_{<i})$ , and under  $\mathcal{H}_1$  we have  $m_i \sim \mathcal{M}_i(X, m_{<i})$ , where  $m_{<i} \triangleq (m_1, \dots, m_{i-1})$ . Concretely, each  $\mathcal{M}_i$  is  $f_i$ -DP with regards to  $X, X'$  for  $f_i$  known in advance, but the actual computation made by  $\mathcal{M}_i$  can depend on  $m_{<i}$  (as long as it is  $f_i$ -DP). We leverage this adaptivity to lower the noise variance in our method’s second step while keeping  $f_2$  fixed (see §3).

We need two more results to define the composition of a sequence of mechanisms. First, Proposition 2.2 in Dong et al. (2019; 2022) shows that for any trade-off function  $f$ , there exist two distributions  $P_f, Q_f$  such that  $T(P_f, Q_f) = f$ . Call any such pair of distributions a representative pair of  $f$ . Second, we define the composition operator  $\otimes$  by  $f \otimes g = T(P_f \times P_g, Q_f \times Q_g)$ . That is, the composition operator between two trade-off functions is the trade-off function between the product distributions on their representative pair. Then Theorem 3.2 in Dong et al. (2019; 2022) shows that:

$$\mathcal{M} : X \rightarrow (\mathcal{M}_1(X), \dots, \mathcal{M}_N(X, y_{<i})) \text{ is } f_1 \otimes \dots \otimes f_N\text{-DP.}$$

Concretely, the mechanism that returns the sequence of results for all compute adaptive  $\mathcal{M}_N$  is  $f_1 \otimes \dots \otimes f_N$ -DP. The previous definitions, as well as this composition result, is what we use to prove Theorem 2.3 and Proposition 2.4.

## B Proofs

**Proposition 2.1 (f-DP Robustness).** *Let  $\mathcal{M} : \mathcal{X} \rightarrow \mathcal{Y}$  be  $f$ -DP for  $B_p(r)$  neighbourhoods, and let  $M_S : X \rightarrow \arg \max_{y \in \mathcal{Y}} \mathbb{P}(\mathcal{M}(X) = y)$  be the associated smooth classifier. Let  $y_+ \triangleq M_S(X)$  be the prediction on input  $X$ , and let  $\underline{p}_+, \overline{p}_- \in [0, 1]$  be such that  $\mathbb{P}(\mathcal{M}(X) = y_+) \geq \underline{p}_+ \geq \overline{p}_- \geq \max_{y_- \neq y_+} \mathbb{P}(\mathcal{M}(X) = y_-)$ . Then:*

$$f(1 - \underline{p}_+) \geq 1 - f(\overline{p}_-) \Rightarrow \forall e \in B_p(r), M_S(X + e) = y_+$$

*Proof.* Let us first consider any runner-up class  $y_-$ . Calling  $M$  the random variable for  $\mathcal{M}$ 's prediction, consider the rejection rule  $\phi = \mathbb{1}\{M = y_-\}$ , where  $\mathbb{1}$  is the indicator function. Denoting  $\alpha \triangleq \mathbb{E}_{\mathcal{M}(X)}(\phi)$ , and using the fact that  $\mathcal{M}$  is  $f$ -DP for  $B_p(r)$  neighbourhoods, we have that  $\forall e \in B_p(r)$ :

$$\begin{aligned} \mathbb{P}(\mathcal{M}(X + e) = y_-) &= \mathbb{E}_{\mathcal{M}(X+e)}(\phi) \\ &\leq 1 - f(\alpha) \leq 1 - f(\overline{p}_-), \end{aligned} \tag{8}$$

where the last inequality is because  $\alpha = \mathbb{E}_{\mathcal{M}(X)}(\phi) = \mathbb{P}(\mathcal{M}(X) = y_-) \leq \overline{p}_-$ , and  $f$  is non-increasing so  $f(\alpha) \geq f(\overline{p}_-)$  and hence  $1 - f(\alpha) \leq 1 - f(\overline{p}_-)$ .

Let us now consider the predicted class  $y_+$ . Keeping the same notations, and defining the rule  $\phi' = \mathbb{1}\{M \neq y_+\} = 1 - \mathbb{1}\{M = y_+\}$ . Then  $\alpha' = \mathbb{E}_{\mathcal{M}(X)}(\phi') = 1 - \mathbb{P}(\mathcal{M}(X) = y_+) \leq 1 - \underline{p}_+$ , and  $\mathbb{E}_{\mathcal{M}(X+e)}(\phi') \leq 1 - f(\alpha') \leq 1 - f(1 - \underline{p}_+)$ , yielding:

$$\begin{aligned} \mathbb{P}(\mathcal{M}(X + e) = y_+) &= 1 - \mathbb{E}_{\mathcal{M}(X+e)}(\phi') \\ &\geq f(1 - \underline{p}_+). \end{aligned} \tag{9}$$

Putting Equations (8) and (9) together, we have that  $\mathbb{P}(\mathcal{M}(X + e) = y_+) \geq f(1 - \underline{p}_+) \geq 1 - f(\overline{p}_-) \geq \mathbb{P}(\mathcal{M}(X + e) = y_-)$  and thus  $m_S(X + e) = y_+$ .  $\square$

Note that we do not have to chose a rule  $\phi \in \{0, 1\}$ , but could instead return any number in  $[0, 1]$ , such as the logits of the base classification model, yielding the following definition for the smoothed classifier  $M_S : X \rightarrow \arg \max_{y \in \mathcal{Y}} \mathbb{E}(\mathcal{M}(X)_y)$ .

**Proposition 2.2 (RS from f-DP).** *Let  $\mathcal{M} : X \rightarrow g(X + z)$ ,  $z \sim \mathcal{N}(0, \sigma^2 \mathbb{I}^d)$ , and  $M_S : X \rightarrow \arg \max_{y \in \mathcal{Y}} \mathbb{P}(\mathcal{M}(X) = y)$  be the associated smooth model. Let  $y_+ \triangleq M_S(X)$  be the prediction on input  $X$ , and let  $\underline{p}_+, \overline{p}_- \in [0, 1]$  be such that  $\mathbb{P}(\mathcal{M}(X) = y_+) \geq \underline{p}_+ \geq \overline{p}_- \geq \max_{y_- \neq y_+} \mathbb{P}(\mathcal{M}(X) = y_-)$ . Then  $\forall e \in B_2(r_X)$ ,  $M_S(X + e) = y_+$ , with:*

$$r_X = \frac{\sigma}{2} (\Phi^{-1}(\underline{p}_+) - \Phi^{-1}(\overline{p}_-)).$$

*Proof.*  $X \mapsto X + z$ ,  $z \sim \mathcal{N}(0, \sigma^2)$  is a Gaussian mechanism. By Equation (2), for the  $B_r(r)$  neighbouring definition, it is  $G_{\frac{r}{\sigma}}$ -DP. By post-processing  $\mathcal{M}$  is also  $G_{\frac{r}{\sigma}}$ -DP.

Applying Proposition 2.1, we have that  $G_{\frac{r}{\sigma}}(1 - \underline{p}_+) \geq 1 - G_{\frac{r}{\sigma}}(\overline{p}_-) \Rightarrow \forall e \in B_2(r)$ ,  $m_S(X + e) = y_+$ . Let us find  $r_X = \sup \{r : G_{\frac{r}{\sigma}}(1 - \underline{p}_+) \geq 1 - G_{\frac{r}{\sigma}}(\overline{p}_-)\}$ . Since  $G_{\frac{r}{\sigma}}(\cdot)$  as a function of  $r$  is monotonously decreasing this will happen at  $G_{\frac{r_X}{\sigma}}(1 - \underline{p}_+) = 1 - G_{\frac{r_X}{\sigma}}(\overline{p}_-)$ , that is:

$$\begin{aligned} \Phi\left(\Phi^{-1}(\underline{p}_+) - \frac{r_X}{\sigma}\right) &= 1 - \Phi\left(\Phi^{-1}(1 - \overline{p}_-) - \frac{r_X}{\sigma}\right) \\ \Rightarrow \Phi^{-1}(\underline{p}_+) - \frac{r_X}{\sigma} &= -\Phi^{-1}(1 - \overline{p}_-) + \frac{r_X}{\sigma} \\ \Rightarrow \Phi^{-1}(\underline{p}_+) - \frac{r_X}{\sigma} &= \Phi^{-1}(\overline{p}_-) + \frac{r_X}{\sigma} \\ \Rightarrow r_X &= \frac{\sigma}{2} (\Phi^{-1}(\underline{p}_+) - \Phi^{-1}(\overline{p}_-)), \end{aligned}$$

where the first implication holds because by symmetry of the standard normal  $1 - \Phi(x) = \Phi(-x)$ , and because  $\Phi$  is strictly monotonous ; the second because similarly,  $\Phi^{-1}(1 - p) = -\Phi^{-1}(p)$ .  $\square$

## C Mask Architecture

Figure 7 shows the architecture of our Mask model  $w(\mathcal{M}_1)$ . We adapt a UNet architecture to preserve dimensions, and use a Sigmoid layer at the end of the model to output values between 0 and 1 for mask weights. We set up our UNet hyperparameters as :  $in\_channels=3$ ,  $out\_channels=1$  (to output a mask),  $base\_channel=32$ ,  $channel\_mult=\{1,2,4,8\}$ .

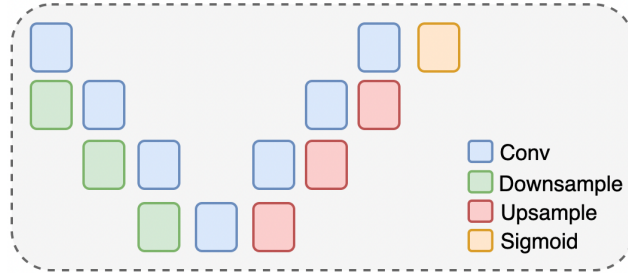


Figure 7: UNet structure



## D Experiment Details

		CIFAR-10	CelebA	ImageNet
GPU		single 24G RTX4090	single 24G RTX4090	single 80G A100
epoch		100	24	100(10+90)
train batch size		256	64	250
test batch size		20	100	25
Mask Model (UNet)	base channel	32	64	16
	optimizer	AdamW	SGD	AdamW
	lr	1e-3	5e-2	1e-3
	weight decay	1e-4	-	-
	momentum	0.9	-	-
	step size	30	100	40
		gamma	1.0	0.5
Base Classifier	model	ResNet110	ResNet50	ResNet50
	optimizer	AdamW	SGD	SGD
	lr	1e-2	5e-2	1e-3
	weight decay	1e-4	-	1e-4
	momentum	0.9	-	0.9
	step size	30	3	30
	gamma	0.1	0.8	0.1

Table 3: Hyperparameters for training ARS.

Table 3 provides the details of our ARS models’ hyper-parameters.

We also tune hyper-parameters for the [Hong et al. \(2022\)](#) baseline on our 20kBG benchmark, focusing on  $\sigma = 0.75$ , at  $k = 48$ . We perform grid search on  $\beta$  (the parameter of the generalized normal distribution for the noise), and find that  $\beta = 2.25$  (close to a Gaussian, but with a wider more and shorted tails) performs best. We also tune other hyper-parameters. In all settings we use training batch size 400, 90 epochs, and Adam optimizer. For the  $\sigma = 0.75, 0.5$  settings we use learning rate 0.001. For the  $\sigma = 0.12, 1.5$  settings we use learning rate 0.0005 with a step learning rate scheduler (30 step size and  $\gamma = 0.2$ ).

## E Additional Results on CelebA

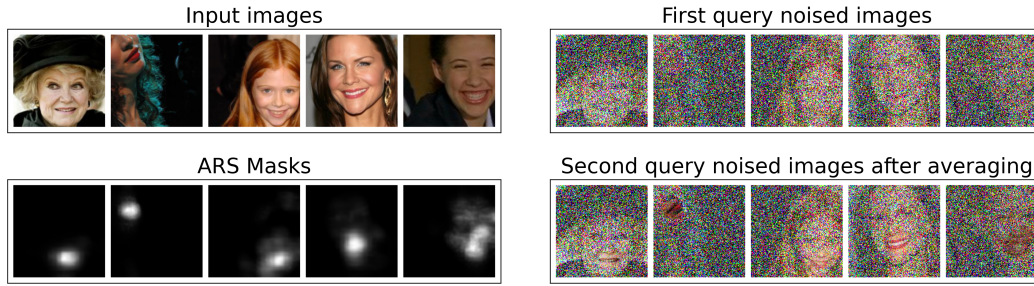


Figure 8: The localized ARS masks produce un-noised mouth regions after averaging.

Figure 8 shows how adaptive masking reduces the noise around areas that are important to classification. The images follow our architecture visualized Figure 1. The mask model is provided the first query noised images as input. The learned masks, presented in the bottom left, are sparse and highly concentrated around the area of interest—the mouth area. The second query noised images (after weighted average) use the mask to clearly reduce the noise around the mouth. This large noise reduction enables ARS to outperform static masking and [Cohen et al. \(2019\)](#), as shown on Figure 4.